Lasers in Manufacturing Conference 2019

Laser Transmission Welding of Thermoplastics – Analytical Model and its Experimental Evaluation

D. Hölzemann[a,b], M. Scholl[a*], U. Russek[a]

[a]*LaborLasertechnik, Rheinische Fachhochschule Köln, Vogelsanger Str. 295, 50825 Köln, Germany*
[b]*now with: Leybold GmbH, Bonner Str. 498, 50968 Köln, Germany*

Abstract

An analytically model for laser transmission welding of thermoplastics will be set up. The local evolution of the temperature field and the formation of the weld joint are modeled in terms of explicit analytical expressions. Necessary approximations will be pointed out keeping computations manageable. The model yields explicit expressions for a process window, weld seam width and depth as well as the tensile strength in terms of the process and materials parameters. The predictions of the model fit well to results obtained from systematic welding experiments. Furthermore, the results show that the analytical model enables a much better understanding of the welding process and allows a much quicker process parameter adaptation within industrial applications.

Keywords: laser welding thermoplastics; analytical model; process parameters; experimental verification;

1. Introduction and Motivation

Theoretical models of manufacturing processes are the basis of process simulations that play an increasingly important role in developing and improving industrial production. As far as laser transmission welding of thermoplastics is concerned these models usually start from physical first principles equations, e.g. heat conduction combined with appropriate boundary conditions and use numerical tools to solve these equations (Acherjee et al., 2012). Often these approaches are restricted to thermal modeling and do not consider the joining process itself (Hopmann & Sooriyapiragasam, 2014). Due to the numerical character of the solutions no statements about the effect of parameter variations can be read of from formulas describing the solutions but require more or less extensive parameter studies. Occasionally more profound insight is obtained from analytical models if these can be found. Analytical models mostly must use significant simplifications of the real situations to provide explicit solutions. Despite they may be considered as toy models they create a deeper understanding and their solutions allow quick and easy estimates to adapt parameters for process applications.

* Corresponding author. Tel.: +49-221-546-879-034;
E-mail address: scholl@rfh-koeln.de.

In this contribution an analytical model for laser transmission contour welding of thermoplastics is set up. After pointing out the chosen approximations, analytical expressions for the temporal and spatial temperature behaviour in the welding zone as well as for the formation of the joint will be developed. Easy analytical evaluability will be one of the central aspects in setting up these expressions. Quantitative predictions for measurable characteristics of the weld will be made. The predictions will be compared with experimental welding results for Polyamide 6 specimens.

2. Description of the Model

2.1. Model Preliminaries

As a basis for modeling the standard arrangement of laser transmission contour welding is assumed as shown in figure 1. A polymer part transparent or translucent for the laser beam is pressed onto a laser absorbent polymer part by an appropriate clamping load (Russek, 2006).

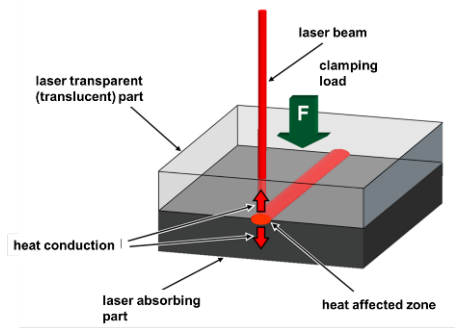

Fig. 1. Standard arrangement of laser transmission contour welding (After: Wikipedia, Laserdurchstrahlschweißen, 2019).

As the laser power density distribution (PDD) moves with constant feed velocity over the surface of the transparent part the beam power is transmitted to the contact plane of the parts and is converted to heat in the absorbent part, where a melt zone is formed. Heat conduction transfers thermal energy into the transparent part, too, and forms a melt zone there. By contact of the melt zones the weld seam is formed that joins the parts after solidification.

For an analytical model description of this process the following assumptions are made (Hölzemann, 2018)

- the contact zone is plane, no pre-weld structure exists
- the PDD of the laser beam is known in the contact zone
- the radius of the PDD is much larger than the optical penetration depth δ_{opt} of the absorbent part
- ideal thermal contact is ensured by the clamping
- apart from the absorbent additive the transparent and the absorbent part are made from same basis thermoplastic material and have equal material parameters, e.g. mass density ρ, specific heat c, thermal conductivity $K$and thus equal thermal diffusivity $\kappa = K/c\rho$
- both welding parts are considered as thick, i.e. they can be treated as semi-infinite as far as heat conduction is concerned; welding of polymer foils or films is excluded
- only heat conduction contributes to heat transport in the material, radiative heat transport is neglected
- there is no melt dynamics, no melt bulges and especially no melt jets appear.

These assumptions turn out to be essential to make the situation simple enough for an analytical modeling.

The results of the model will be examined with respect to these assumptions.

2.2. Thermal modeling

Using the theory of partial differential equations (Morse & Feshbach, 1953) it is possible to find an analytically solvable integral equation for the temperature field of the heat source distribution caused by laser absorption in the absorbent part. This solution strategy is not followed here. The results turn out to be too involved to unravel an underlying structure and to allow simple evaluation with respect to observable quantities like e.g. the weld seam section and its dimensions. However, the results show that the temperature dependence with respect to the *z*-direction is approximately described by functions that do not differ very much from the fundamental solution of the heat equation. This motivates the following more physically minded phenomenological approach using the fundamental solution (Green's function) of the heat equation.

To start with, it is assumed that irradiation has produced an infinitesimally thin laterally constant surface heat energy density $dQ/dxdy$ concentrated in a layer at $z = z_0$. For generality the position z_0 may differ slightly from the contact plane of figure 1 which is defined at $z = 0$. The spatiotemporal spreading of the heat energy in vertical direction z can be described by a Gaussian temperature distribution which is the fundamental solution of the heat equation. As the low temperature wings of the Gaussian are not essential for the welding process the Gaussian is approximated by a triangular distribution for the temperature increase $\Delta T(z,t) = T(z,t) - T_{ambient}$. The function reads (Hölzemann 2018)

$$\Delta T(z,t) = \frac{dQ/dxdy}{c\,\rho\,\delta(t)} \cdot \Theta\left(1 - \frac{|z - z_0|}{\delta(t)}\right) \cdot \left(1 - \frac{|z - z_0|}{\delta(t)}\right) = \frac{dQ/dxdy}{c\,\rho\,\delta(t)} \cdot \left[1 - \frac{|z - z_0|}{\delta(t)}\right] \qquad (1)$$

with the thermal parameters ρ_M, c, κ assumed the same in both parts as outlined in section *2.1.* The symbol $\Theta(x)$ stands for the Heaviside Theta function which equals 0 for $x < 0$ and takes the value 1 for $x \geq 0$. The square brackets stand as abbreviation for $[x] = x \cdot \Theta(x)$ and correspond to the Föppl- or Macaulay-brackets used elsewhere in engineering (Wikipedia, Macaulay Brackets, 2019). $\delta(t) = \sqrt{8\kappa t}$ describes the time dependent half width of the triangle and is identical to the thermal penetration depth (Morse & Feshbach, 1953). $\delta(t)$ vanishes when time approaches zero and the temperature increase ΔT approaches infinity at $z = z_0$ and zero everywhere else.

Inserting modifications and appropriate expressions for $\delta(t), z_0, dQ/dydy$ the function (1) can adapted to describe the temperature distribution for contour welding in a surprisingly reasonable way. First, substituting $t \to t + t_V$ in $\delta(t)$ the initial surface heat energy density at $t = 0$ is present not in an infinitesimally thin layer but spread over thickness δ_0 around the layer at $z = z_0$. The t_V is a virtual lead time that must be determined from the condition $\delta(t = 0) = \delta_0$ yielding

$$t_V = \frac{\delta_0^2}{8\kappa} \qquad (2)$$

A modified width $\delta^2(t) = \delta_0^2 \cdot (1 + t/t_V)$ is found. The virtual lead time t_V characterizes the rate of increase of the width $\delta(t)$.

By these simple substitutions the temperature function now describes the temperature development starting from a triangular initial distribution *after* but not *during* laser irradiation. It turns out, however, that for the usual feed velocities in contour welding the irradiation time is of the same order of magnitude as the virtual lead time t_V. Thus it is a reasonable approximation to treat heat conduction as if it appears after irradiation and to neglect further modifications.

Note that with insertion of t_V in $\delta(t)$ the initial temperature distribution of eq. (1) has a symmetric triangular *z*-dependence. This does not fit very well the asymmetric exponential *z*-dependence of the volume heat power density enforced by Beer's absorption law with optical penetration depth δ_{opt}. Nevertheless the

triangular form will be kept for simplicity. By choosing $\delta_0 = \delta_{opt}$ and $z_0 = 0.49 \cdot \delta_{opt} \approx \delta_{opt}/2$ the average quadratic deviation between the triangular and the exponential distribution is minimized and for further consideration these values will be used. It is clear already at this point that the model will not be able to reproduce e.g. weld seam sections that are asymmetric with respect to the *z*-direction

In a standard set up for contour welding of plastics the contact plane surface heat energy density $dQ/dxdy$ in (1) is generated by a uniformly moving circularly symmetric laser PDD with radius w. As usually the relation $w \gg \delta_{opt}$ holds the typical time t_V, eq. (2), for heat conduction into the depth of the material is much shorter than the analog time constant t_w for heat conduction into the transverse direction. One finds $t_w/t_V = w^2/\delta_{opt}^2$. Common values $w \geq 1\ \mathrm{mm}$ and $\delta_{opt} \leq 0.1\ \mathrm{mm}$ yield $t_w/t_V \approx 100$. This implies that the weld is formed due to heat conduction into the depth before lateral heat conduction must be taken into account. Lateral spreading of the temperature can be neglected and (1) suffices to describe heat conduction.

The boundary of a circular PDD of radius w moving with feed velocity v over the contact plane to positive y-direction is represented by a moving circle $x^2 + (y - v \cdot t)^2 = w^2$. Solving this equation for t the instant t_B for the begin and the instant t_E for the end of irradiation by the laser beam can be computed for any given position (x, y) on the surface. The results for $t_{B/E}$ read

$$t_{B/E}(x,y) = \frac{y}{v} \pm \frac{w}{v} \cdot \sqrt{1 - x^2/w^2} \approx \frac{y}{v} \pm \frac{w}{v} \cdot \left(1 - \frac{g}{2} \cdot x^2/w^2\right) \tag{3}$$

The use of the quadratic approximation with $g \approx 1.37$ for the root avoids for all x that imaginary times occur. This substitution is justified as the difference between the root and its approximation becomes relevant only for $x \geq w$ where the power density values of the corresponding PDD become negligible, i.e. no power is irradiated there. Corresponding to the varying instants of irradiation the previous expressions for the width function $\delta(t)$ must be modified to yield

$$\delta^2(t) = \delta_{opt}^2 \cdot \left(1 + \frac{t - t_B(x,y)}{t_V} \cdot \Theta\big(t - t_B(x,y)\big)\right) = \delta_{opt}^2 \cdot \left(1 + \left[\frac{t - t_B(x,y)}{t_V}\right]\right) \tag{4}$$

(remember $\delta_0 = \delta_{opt}$). The Theta function has to be inserted in (5) to maintain causality so that the spreading starts exactly with the begin of irradiation and no effects occur before. Again the previously introduced Macaulay bracket notation is used.

The final step that has to be taken is to substitute the naïve constant surface heat energy density $dQ/dxdy$ by the appropriate expression $dQ(x,y,t)/dxdy$ involving the PDD $I(x, y - v \cdot t)$ moving across the contact plane. For a general PDD this is

$$\frac{dQ(x,y,t)}{dxdy} = \int_0^t I(x, y - v \cdot t')\, dt' = \frac{1}{v} \cdot \int_{y - v \cdot t}^{y} I(x, y')\, dy' \tag{5}$$

For Gaussian PDD $I(x,y) = 2\,P/\pi w^2 \cdot \exp\{-2\,(x^2 + y^2)/w^2\}$ where P and w stand for power and radius of the PDD the integral can be done in terms of error functions obtaining

$$\frac{dQ_G(x,y,t)}{dxdy} = \frac{P}{\sqrt{2\pi}\, w\, v} \cdot e^{-2\,x^2/w^2} \cdot \left(\operatorname{erf}\sqrt{2}\frac{y}{w} + \operatorname{erf}\sqrt{2}\frac{v \cdot t - y}{w}\right) \tag{6}$$

Plugging all ingredients in equations (5,6) as well as (4), (3) and (2) into equation (1) a closed formula for the temperature distribution will result. This, however, relies on temperature independent parameters for mass density, specific heat and thermal diffusivity. Whereas this is satisfied approximately for the mass density it is known from thermal analysis that neither specific heat nor thermal diffusivity are temperature independent. In addition fusion enthalpy must be taken into account for partially crystalline polymers. In order to cope with the temperature dependencies of the specific heat the full temperature range for welding

is divided in the range *R1* between ambient and melting temperature $0 \leq \Delta T_1 < \Delta T_M$ with the average specific heat c_s of the solid state and the temperature range *R2* between melting and at most degradation temperature $\Delta T_M \leq \Delta T_2 < \Delta T_Z$ with the specific heat c_l of the liquid state in *R2*. From differential scanning calorimetry measurements a reasonable value of c_s can be estimated. The value of c_l, however, is prone to higher uncertainty especially as the upper temperature of *R2* is not exactly known. As c enters linearly the temperature distribution is subject to a corresponding degree of uncertainty. The dependence on thermal diffusivity κ is weaker in the root of $\delta(t)$. Here an average value over the total temperature range is used.

For the temperature range *R1* the previous equations can be used to find an explicit temperature distribution $\Delta T_1(x, y, z, t)$. For the temperature range *R2* a second temperature distribution $\Delta T_2(x, y, z, t)$ is computed taking the melting temperature as reference and using c_l. The amount of energy necessary to heat the polymer to melting temperature as well as the fusion enthalpy h_M are considered separately.

It is clearer to represent these temperature distributions in dimensionless scaled coordinates and quantities.

Defining normalized temperatures as

$$\vartheta_{1,2} = \frac{\Delta T_{1,2}}{T_M - T_{ambient}} \tag{7}$$

with T_M the melting temperature and dimensionless scaled coordinates as

$$\tilde{x} = \frac{x}{w}, \quad \tilde{y} = \frac{y}{w}, \quad \tilde{z} = \frac{z}{\delta_{opt}} \qquad \tilde{t} = \frac{t}{w/v} \tag{8}$$

the temperature distributions resulting from a Gaussian PDD read (Hölzemann, 2018)

$$\vartheta_1(\tilde{x}, \tilde{y}, \tilde{z}, \tilde{\eta}) = \sqrt{2\,\pi}\,\frac{\gamma}{\alpha}\,\Theta(\tilde{t})\,e^{-2\tilde{x}^2}\,\left(\operatorname{erf}\left(\sqrt{2}\tilde{y}\right) + \operatorname{erf}\left(\sqrt{2}\tilde{\eta}\right)\right)\,\frac{1}{\tilde{\delta}(\tilde{x}, \tilde{\eta})}\,\left[1 - \frac{|\tilde{z} - \frac{1}{2}|}{\tilde{\delta}(\tilde{x}, \tilde{\eta})}\right]$$

$$\vartheta_2(\tilde{x}, \tilde{y}, \tilde{z}, \tilde{\eta}) = \sqrt{2\,\pi}\,\gamma\,\Theta(\tilde{t})\,e^{-2\tilde{x}^2}\,\left(\operatorname{erf}\left(\sqrt{2}\tilde{y}\right) + \operatorname{erf}\left(\sqrt{2}\tilde{\eta}\right)\right)\,\frac{1}{\tilde{\delta}(\tilde{x}, \tilde{\eta})}\,\left[1 - \frac{|\tilde{z} - \frac{1}{2}|}{\tilde{\delta}(\tilde{x}, \tilde{\eta})}\right] + \Gamma \tag{9}$$

with

$$\tilde{\delta}(\tilde{x}, \tilde{\eta}) = \sqrt{1 + \frac{8}{\widetilde{Pe}} \cdot \left[\tilde{\eta} + 1 - \frac{g}{2}\,\tilde{x}^2\right]} \quad , \quad \tilde{\eta} = \tilde{t} - \tilde{y} \tag{10}$$

and

$$\gamma = \frac{1}{2\pi} \cdot \frac{\frac{P}{w\,v\,\delta_{opt}}}{c_l\,\rho\,(T_M - T_A)} \quad , \quad \widetilde{Pe} = \frac{\delta_{opt} \cdot v}{\kappa \cdot w} \quad , \quad \alpha = \frac{c_s}{c_l} \quad , \quad \Gamma = 1 - \frac{c_s}{c_l} - \frac{h_m}{c_l\,(T_M - T_A)} \tag{11}$$

In the present form the temperature distributions are expressed in terms of simple elementary and special functions depending on scaled variables. The variable $\tilde{t}$ that measures time in multiples of the interval necessary for the beam to cover the PDD radius w, the transverse coordinates $\tilde{x}, \tilde{y}$ measure the lateral position in multiples of the beam radius w and the longitudinal depth $\tilde{z}$ is given in multiples of the optical penetration depth δ_{opt}. The parameters may be grouped in *process* parameters P, w, v and δ_{opt} which are at hand for the optimization of the manufacturing result and *materials* parameters $\rho, c_l, c_s, K, \kappa, T_M, T_A$ and melting enthalpy h_M. The temperatures (9) depend on these parameters only via four *model* parameters $\gamma, \widetilde{Pe}, \alpha$ and Γ. The process parameters merely enter in $\gamma, \widetilde{Pe}$, so only these two parameters are at hand for process optimization. Physically γ is a dimensionless measure for the process energy density as the numerator of γ in (11) is an approximation for the energy density the beam leaves in the absorbent part. $\widetilde{Pe}$ is a modified form of the Peclet number which gives a dimensionless measure for the feed velocity v.

The above expressions may be used to generate plots of the temperature fields. As the plot only gives a static two dimensional representation time and one spatial variable have to be fixed. For the example plot of the temperature track in the weld seam the combination $\tilde{t} = 20$ and $\tilde{z} = 0$ are chosen. Thus the plot

represents the lateral temperature distribution in the contact plane after the beam has moved 20 beam radii after begin of irradiation. For definiteness the model parameters $\gamma = 2.38, \widetilde{Pe} = 1.57, \alpha = 0.65$ and $\Gamma = 0.27$ were chosen for the plot. For temperatures lower than the melting temperature, i.e. $\vartheta \leq 1$ the function ϑ_1 must be used and ϑ_2 for higher temperatures. Consequently two isothermal lines will be found for the melting temperature $\vartheta = 1$, cf. the red and green lines in the plot. The area between these isothermal lines must be interpreted as the melting or solidification zone where solid and liquid phases coexist.

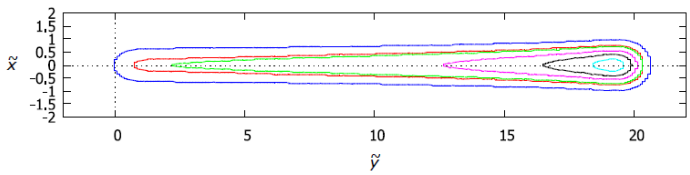

Fig. 2. Isothermal plot of computed temperature distribution in weld seam. From outside to inside the isothermal lines are $\vartheta_1 = 0.5; 1.0$ and $\vartheta_2 = 1.0; 1.33; 1.66;\ 2.0$ (Hölzemann, 2018)

Lots of information can be obtained from plots like figure 2. For a given isothermal line the length of a section at some $\tilde{x}$ is identical to the time interval in which the corresponding temperature is exceeded. The maximum width of the isothermals allows to identify the maximum temperature reached at some point. However, analytical expressions can be found for all these quantities.

2.3. Model of for joining process

Unfortunately there is no generally accepted model for the formation of the weld joint that allows to estimate its tensile strength σ. Here a phenomenological approach is chosen. This approach has to describe the fact that the tensile strength of some point in a weld joint takes the value zero if the maximum temperature ϑ_{max} acquired during the thermal history of this point is less than the welding temperature (i.e. for $\vartheta_{max} < 1$). If higher maximum temperatures are reached the tensile strength varies to some maximum value. As in an optimal weld the tensile strength approaches the value σ_B of the bulk material, so we assume that the maximum obtainable value is $\sigma/\sigma_B = 1$. Finally σ goes to zero again for temperatures higher than the approximate degradation temperature (i.e. for $\vartheta_{max} > n \cdot \vartheta_Z$). ϑ_Z is the degradation temperature found from e.g. thermogravimetric measurements and n some number estimated to $1 \leq n \leq 3$ The maximum temperature at a point in the weld must be found from the temperature functions of the previous section. From the discussed temperature ranges only the function ϑ_2 can be relevant, so $\vartheta_{max} = \vartheta_{2,max}$. The simplest ansatz satisfying the described behavior is a parabola given by

$$\frac{\sigma}{\sigma_B} = \frac{4}{(n \cdot \vartheta_Z - 1)} \cdot (\vartheta_{2,max} - 1) - \frac{1}{(n \cdot \vartheta_Z - 1)} \cdot (\vartheta_{2,max} - 1)^2 \qquad (12)$$

More exactly the formation of the tensile strength at some point will not depend on the maximum temperature alone but depend on the entire temperature history. However, parameters like e.g. the temperature holding time are neglected. Further it is assumed that the clamping pressure is chosen optimally. Hence no dependence on further parameters needs to be considered and the simplified description of (12) may be applied.

Note that the maximum temperature appearing in (12) will be a function of the coordinates $\vartheta_{2,max}(\tilde{x}, \tilde{z})$. If this function is inserted into the expression (12) a coordinate dependent tensile strength $\sigma(\tilde{x})$ results. Figure (3) shows an example where a Gaussian temperature dependence on $\tilde{x}$ was used. The result may

display a central decrease in the local tensile strength. This is due to the fact that the maximum temperature of the Gaussian is higher than the temperature where the tensile strength function (12) reaches its maximum. If - even worse - the strength decreases to zero in the center degradation will be visible in the middle of the weld seam.

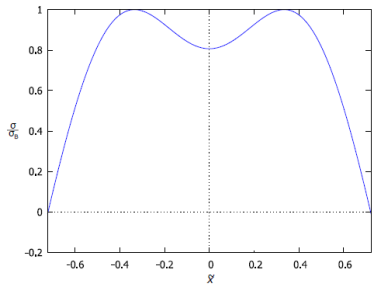

Fig. 3. Local tensile strength in a section of the weld seam produced with a Gaussian PDD according to equation (12) (Hölzemann, 2018)

In tensile tests merely the average strength $\bar{\sigma}$ of the joint can be measured. From the local strength found from (12) this calculated by

$$\bar{\sigma} = \frac{\int_{-\tilde{x}_0}^{+\tilde{x}_0} \sigma(\tilde{x})\, d\tilde{x}}{2\,\tilde{x}_0} \tag{13}$$

where $\tilde{x}_0$ is the half width of weld seam in the contact plane. Note that due to averaging the average tensile strength takes smaller values than the maxima of the local strength.

3. Theoretical analysis of the model

In this section some results that may be derived from the previous equations will be presented. The expressions (9) allow the calculation of the temperatures at an arbitrary time and position. This is not necessary in general as mostly positions reasonably distant from the start and thus much later than $t = 0$ are considered. In this case the Theta functions in (9) may be omitted and the first error function in the brackets, respectively, can be substituted by unity which is its asymptotical value for large argument. These asymptotic temperature functions depend on time $\tilde{t}$ and the feed motion coordinate $\tilde{y}$ only in the combination $\tilde{\eta} = \tilde{t} - \tilde{y}$. The plots of the temperature distributions tracks look very much like in figure 2 as regards the rapidly heating head of the track. Differences appear in the trail which will be more extended.

The asymptotic functions simplify the following computations a lot. As an example the maximum values of the temperature history of the distributions are found from determining the extremum with respect to $\tilde{t}$ and thus to $\tilde{\eta}$. The result consequently does no longer depend on $\tilde{\eta}$. To a good approximation these maxima are obtained by inserting $\tilde{\eta} = 1$ into the asymptotic functions. As $\tilde{\eta} = \tilde{t} - \tilde{y} = 0$ corresponds to the position of the PDD center in a co-moving coordinate system $\tilde{\eta} = 1$ is located one beam radius behind the center, i.e. the rear boundary of the PDD where the irradiation just has terminated. The resulting expressions read

$$\vartheta_{1,max}(\tilde{x},\tilde{z}) = 2\sqrt{2\,\pi}\,\frac{\gamma}{\alpha}\,e^{-2\tilde{x}^2}\,\frac{1}{\tilde{\delta}_{max}(\tilde{x})}\left[1-\frac{\left|\tilde{z}-\frac{1}{2}\right|}{\tilde{\delta}_{max}(\tilde{x})}\right]$$

$$\vartheta_{2,max}(\tilde{x},\tilde{z}) = 2\sqrt{2\,\pi}\,\gamma\,e^{-2\tilde{x}^2}\,\frac{1}{\tilde{\delta}_{max}(\tilde{x})}\left[1-\frac{\left|\tilde{z}-\frac{1}{2}\right|}{\tilde{\delta}_{max}(\tilde{x})}\right]+\Gamma \qquad \text{with} \quad \tilde{\delta}_{max}(\tilde{x}) = \sqrt{1+\frac{16}{\widetilde{Pe}}\left[1-\frac{g}{4}\,\tilde{x}^2\right]} \tag{14}$$

From functions (14) the isothermal lines of the maximally acquired temperature in a section of the weld seam are determined. Fig. 4 shows a plot

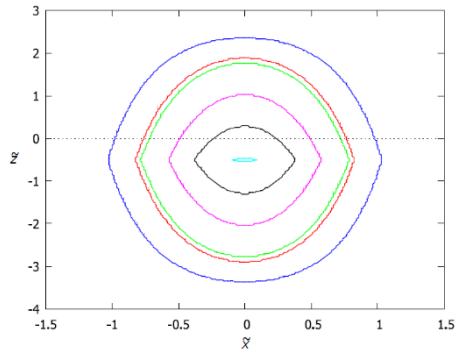

Fig.4. Contour Plot of the maximally acquired temperatures in a section of the weld seam. From outside to inside the isothermal lines are $\vartheta_{1,\max} = 0.5; 1.0$ and $\vartheta_{2,\max} = 1.0; 1.5; 2{,}0;\ 2.5$. Parameter values as in Fig.1 (Hölzemann, 2018)

The contours of the maximally acquired temperatures in a section of the weld seam can be checked experimentally from microscopic sections of the seam. In these sections the melt zone is visible from changes in the morphology of the partially crystalline thermoplastic. Thus the isothermal of the maximum temperature $\vartheta_{max} = 1.0$ can be compared with experiment. Especially the maximum lateral width $\tilde{x}_{max}$ of the seam, the width $\tilde{x}$ in the contact plane at $\tilde{z} = 0$ and the thickness $\Delta\tilde{z}_{max}$ at coordinate $\tilde{x} = 0$ can be compared quantitatively. Here only the expression for $\Delta\tilde{z}_{max}$ is quoted. It can be calculated analytically without approximation as

$$\Delta\tilde{z}_{max} = 2 \cdot \sqrt{1 + \frac{16}{\widetilde{Pe}}} \cdot \left(1 - \frac{1}{2\sqrt{2\,\pi}} \cdot \frac{1-\Gamma}{\gamma} \cdot \sqrt{1 + \frac{16}{\widetilde{Pe}}}\right) \tag{15}$$

The equations for the widths $\tilde{x}_{max}, \tilde{x}$ can be solved in an analytic approximation but will not be presented explicitly. All these expressions depend on the (dimensionless) process energy density and the Peclet number as well as on the thermal parameter Γ that are determined from (11) and the parameters of the material and the process as they are used in manufacturing.

Finally the temperature $\vartheta_{2,max}$ from equation (14) enters the determination of the tensile strengths in (12) and (13). The experimentally relevant result for the average tensile strength again yields an approximate analytical expression not to be quoted here. The result is presented in the plot of figure 5 with the average tensile strength as function of process power density and Peclet number.

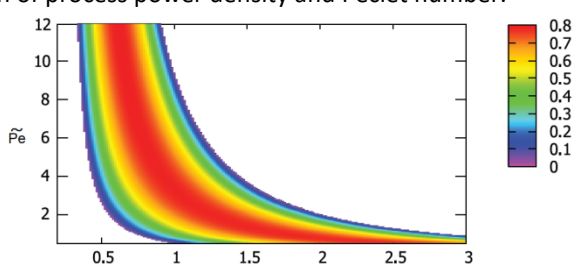

Fig. 5. Average tensile strength as function of process power density and Peclet number. Material parameters for PA 6. (Hölzemann, 2018)

Note that the plot represents the process window for contour welding. All model parameter combinations $(\gamma, \widetilde{Pe})$ fitting the band of nonvanishing tensile strength will lead to a weld joint. Note further that fixing the model parameters to some pair of values inside the band does not determine the process parameters P, w, v and δ_{opt} uniquely as many combinations these process parameters lead to the same model parameters.

4. Experimental evaluation of the model

The model predictions of the previous section as well as numerous additional predictions have been checked with welding experiments for PA6. The thermal properties of the material as used for the calculations are found in appendix A. The welds were performed using a *G4 50W Fibre-Laser* by *SPI Inc*. The laser works at $\lambda = 1064\ \mathrm{nm}$ with an $M^2 \approx 1$ so that anywhere along a beam caustic the PDD is ensured to be Gaussian. Hence different beam radii can be chosen. A weld seam of length $l = 20\ \mathrm{mm}$ is manufactured between two flat test pieces from transparent PA6 and PA6 with carbon black and a measured penetration depth $\delta_{opt} = 59.1\ \mu\mathrm{m}$. The values of the model parameters $\gamma, \widetilde{Pe}$ as computed from the process and thermal parameters are shown in table 1.

Table 1. Model parameters $\gamma, \widetilde{Pe}$ as used in the experiments, computed from the process parameters $P, v, w. \delta_{opt}$ and the thermal parameters, cf. appendix, with formulae (11) (Hölzemann, 2018).

P	W	20,92	22,32	26,42	35,22	30,91	33,29
v	$\frac{\mathrm{mm}}{\mathrm{s}}$	13,99	22,38	31,43	78,57	158,24	172,84
w	mm	1,916	1,916	1,076	1,076	0,834	0,74
δ_{opt}	µm	59,1	59,1	59,1	59,1	59,1	59,1
$\widetilde{Pe}$	-	0,39	0,63	1,57	3,92	10,19	12,55
γ	-	2,38	1,59	2,38	1,27	0,714	0,793

The results of the experimental evaluation of the maximum width $\tilde{x}_{max}$ of the weld seam, the width $\tilde{x}$ in the contact plane and the thickness of the weld seam are presented in table 2.

Table 2. Comparison of experimental results and theoretical predictions for the maximum width $\tilde{x}_{max}$ of the weld seam, the width $\tilde{x}$ in the contact plane and the thickness $\Delta\tilde{z}_{max}$ of the weld seam in respective scale units (Hölzemann, 2018).

$\widetilde{Pe}$	γ	$\tilde{x}$			$\tilde{x}_{max}$			Δz		
		Modell	Experiment	Dev. in %	Modell	Experiment	Dev. in %	Modell	Experiment	Dev. in %
0,39	2,38	1,362	1,391	+2,13	1,502	1,527	+1,66	7,823	4,785	-38,83
0,63	1,59	1,209	1,053	-12,9	1,381	1,285	-6,95	5,441	3,091	-43,19
1,57	2,38	1,728	1,719	-0,52	1,883	1,911	+1,49	5,321	4,43	-16,74
3,92	1,27	1,519	1,475	-2,9	1,74	1,788	+2,76	3,343	2,57	-23,12
10,20	0,71	1,239	1,013	-18,24	1,568	1,442	-8,04	2,152	1,624	-24,54
12,55	0,79	1,343	1,328	-1,12	1,665	1,754	+5,35	2,178	1,516	-30,39

The last group of results is for the experimental and theoretical tensile strength contained in table 3.

Table 3. Comparison of experimental results and theoretical predictions for the tensile strengths (Hölzemann, 2018).

	$\widetilde{Pe}$	γ	Modell $\frac{\sigma}{\sigma_B}$	Experiment $\frac{\sigma}{\sigma_B}$	Deviation in %
3.1	0,39	2,38	0,708	0,63	-11,0
3.2	0,63	1,59	0,569	0,704	+19,0
3.3	1,57	2,38	0,467	0,604	+22,7
3.4	3,92	1,27	0,772	0,766	- 8,0
3.5	10,20	0,71	0,651	0,64	- 1,7
3.6	12,55	0,79	0,0,732	0,761	+ 3,6

Disregarding the results for $\Delta\tilde{z}_{max}$for the moment the results show a satisfactory agreement between theoretical predictions and experimental results. This may be not too surprising for the lateral widths $\tilde{x}_{max}$ and $\tilde{x}$ as heat conduction plays only a minor role for them. In contrast to the simplicity of the approach this is a real surprise, however, for the values of the tensile strength. The results for $\Delta\tilde{z}_{max}$ which is highly sensible to heat conduction all experimental value are systematically smaller than the theoretical expectation. This leads to the conclusion that the temperature diffusivity has been chosen to big and the deviations may vanish if a more appropriate value is chosen.

5. Conclusion and outlook

Despite the vast assumptions and simplifications that have been made in setting up the analytical model promising results have been obtained from comparison with experiment. Mostly the agreement with experiment is satisfactory. A crucial point is the choice of adequate average values for the temperature dependent material properties.

On top of the shown examples quantitative analytical equations for many other potentially interesting parameters can be found from the model. Most interesting the effect of the PDD shape may be studied quantitatively with the model. Experimentally the validity for other polymers must be tested. If the results are comparably successful there the model will provide an easily usable tool for parameter estimates and process preparation.

References

Acherjee, Bappa ; Kuar, Arunanshu S. ; Mitra, Souren ; Misra, Dipten, 2012. Modeling of laser transmission contour welding process using FEA and DoE. In: Optics & Laser Technology 44, S. 1281–1289.

Hopmann, C.; Sooriyapiragasam, S., 2014. Prozessmodellierung des Erwärmvorgangs beim Laserdurchstrahlschweißen von Kunststoffen In:Joining Plastics. Fügen von Kunststoffen, Nr. 3/4 2014, S. 170–177.

Wikipedia, Laserdurchstrahlschweißen, 2019, Von MathiasW82 - Eigenes Werk, CC BY-SA 3.0, https://commons.wikimedia.org/w/index.php?curid=16042811

Russek, Ulrich A., 2006. Prozesstechnische Aspekte des Laserdurchstrahlschweißens von Thermoplasten, Diss. RWTH Aachen

Morse, P.M.; Feshbach, H., 1953. Methods of Theoretical Physics, Part 2, Ch. 12 Diffusion, Wave Mechanics, pp. 1584 ff., Mc Graw Hill Book Company 1953.

D. Hölzemann, 2018. Experimentelle Überprüfung des Einflusses der Prozessparameter auf das Schweißergebnis beim Konturschweißen im Rahmen eines analytischen Prozessmodells, Master Thesis, Rheinische Fachhochschule Köln, Dec. 2018.

Wikipedia, Macaulay Brackets, 2019. https://en.wikipedia.org/wiki/Macaulay_brackets

Appendix. Thermal Properties of PA6

Table 4. Thermal properties of PA 6 as used for the calculations (in german) (Hölzemann, 2018).

	Formelzeichen	Einheit	Wert
Schmelztemperatur	T_M	°C	219,78
		K	492,93
Glasübergangstemperatur	T_G	°C	51,46
		K	324,61
Umgebungstemperatur	T_A	°C	25,0
		K	298,15
Zersetzungstemperatur	T_Z	°C	706,73
		K	979,88
spez. Wärmekapazität, fest	c_s	$\frac{J}{g \cdot K}$	2,8
spez. Wärmekapazität, flüssig	c_l	$\frac{J}{g \cdot K}$	4,3
Schmelzenthalpie	h_m	$\frac{J}{g}$	62,69
Dichte, mittlere	$\overline{\rho}$	$\frac{g}{mm^3}$	0,00106
Wärmeleitfähigkeit, fest	K_s	$\frac{W}{mm \cdot K}$	0,00026
Wärmeleitfähigkeit, flüssig	K_l	$\frac{W}{mm \cdot K}$	0,00018
Temperaturleitfähigkeit, mittlere	$\overline{\kappa}$	$\frac{mm^2}{s}$	0,065